Original Article

Deep learning for the identification of pre- and post-capillary pulmonary hypertension on cine MRI

Kai Lin, Roberto Sarnari, Ashitha Pathrose, Daniel Z. Gordon, Michael Markl, James C. Carr

Department of Radiology, Northwestern University, Chicago, IL, USA

Contributions: (I) Conception and design: K Lin; (II) Administrative support: M Markl, JC Carr; (III) Provision of study materials or patients: K Lin, A Pathrose, R Sarnari; (IV) Collection and assembly of data: K Lin, A Pathrose, DZ Gordon, R Sarnari; (V) Data analysis and interpretation: K Lin, A Pathrose, DZ Gordon, R Sarnari; (VI) Manuscript writing: All authors; (VII) Final approval of manuscript: All authors.

Correspondence to: Kai Lin, MD, MS. Department of Radiology, Northwestern University, 737 N Michigan Avenue, Suite 1600, Chicago, IL 60611, USA. Email: kai-lin@northwestern.edu.

Background: The aim of the present study was to develop a deep learning (DL) framework that can identify elevated left heart pressure in pulmonary hypertension (PH) based on cine MRI-derived left ventricular (LV) motion/deformation patterns.

Methods: Fifty-four PH patients (23 males, 58.9±13.5 years old) were retrospectively included in the present study. Heart deformation analysis (HDA) was applied to acquire LV displacement, velocity strain and strain rate on cine MRI datasets. Peak values of motion/deformation indices at early and late diastole entered an artificial neural network (ANN), which was developed with Python, to discriminate cases of pre-capillary PH [defined as mean pulmonary arterial pressure (mPAP) ≥25 mmHg and pulmonary capillary wedge pressure (PCWP) ≤15 mmHg] from post-capillary PH (mPAP ≥25 mmHg and PCWP >15 mmHg).

Results: Cine MRI datasets of 54 PH patients were eligible for HDA processing. Peak radial and circumferential displacement, velocity and strain rates in systole, early and late diastole were extracted. The ANN model was fit and trained with cine MRI-derived indices from 40 randomly chosen PH patients. Then, the model successfully identified the type of PH in the remaining 14 patients. The accuracy, sensitivity, specificity, positive predictive value (PPV) and negative predictive value (NPV) to discriminate post-capillary PH from pre-capillary PH were 86%, 83%, 88%, 83% and 88%, respectively. The area under the curve (AUC) of the receiver operating characteristic (ROC) curve was 0.85 [95% confident interval (CI): 0.629–1].

Conclusions: DL can identify elevated left heart pressure underlying post-capillary PH based on LV motion/deformation patterns presented on regular cine MRI datasets.

Keywords: Deep learning (DL); heart deformation analysis (HDA); pulmonary hypertension (PH); left heart pressure

Received: 29 August 2021; Accepted: 06 January 2022; Published: 30 March 2022.

doi: 10.21037/jmai-21-27

View this article at: https://dx.doi.org/10.21037/jmai-21-27

Introduction

Elevated left heart pressure is a major manifestation of left heart dysfunctions. Although pulmonary capillary wedge pressure [PCWP; measured by using the right heart catheterization (RHC)] and left ventricular (LV) end-diastolic pressure [LVEDP; measured by using the left heart catheterization (LHC)] are most frequently used surrogate measurements for the estimation of left heart pressure, RHC and LHC are invasive procedures and cannot be regularly applied in many patients due to possible side effects (1). Therefore, noninvasive approaches for the estimation of the left heart pressure is highly desired for the diagnosis of multiple cardiothoracic disorders with LV involvements, such as heart failure (HF) with preserved ejection fraction (HFpEF) and post-capillary pulmonary hypertension (PH) (2).

Cine MRI is the "standard of care" for detecting HF by measuring LV ejection fraction (LVEF) and LV mass (LVM) in clinical practice (3,4). Additionally, cine MRI datasets also contain detailed information regarding LV motion and deformation patterns that can be represented by using biomechanics parameters, such as displacement, velocity strain and strain rate. Those LV motion/deformation indices at major directions of cardiac motions, can be extracted from regular cine MRI datasets by using highly automated image processing tools, such as heart deformation analysis (HDA) (5-7). The levels of those indices have been found to linearly associate with the PCWP in the context of PH (8). However, there were no well-accepted criteria for multiple motion/deformation indices in defining "normal" and "abnormal" LV functions. Additionally, many motion/deformation indices, despite their different definitions, which could correlate to each other, should be taken into account. As a result, it is still challenging to judge increased left heart pressure based on cine MRI.

Recently, artificial intelligence (AI) has become a promise method for increasing the accuracy of diagnosis and the efficiency of clinical decision-making under complicated clinical situations (9). Deep learning (DL) is an AI function that has been widely used in radiology for processing medical images. We hypothesized that DL might facilitate the interpretation of multiple LV motion/deformation indices in the diagnosis of LV abnormalities. Therefore, the aim of the present study was to develop a DL framework to identify elevated left heart pressure in PH based on cine MRI-derived LV motion/deformation patterns. We present the following article in accordance with the STARD reporting checklist (available at https://jmai.amegroups.com/article/view/10.21037/jmai-21-27/rc).

Methods

Patient population

This is a retrospective study with a cross-sectional design. The study was conducted in accordance with the Declaration of Helsinki (as revised in 2013). The study was approved by the institutional review board of Northwestern University (STU00205106). Written informed consents were provided by all participants. From 2015 to 2020, 54 consecutive PH patients (diagnosed with RHC; 23 males; 58.9±13.5 years old; range, 32–89 years old) were recruited for a cardiac MRI scan. These PH patients were reported in a previous publication demonstrating that multiple cine MRI-derived LV motion/deformation indices were significantly different between patients with pre- and post-capillary PH (8). In the present study, we reported a novel DL application on the diagnosis of these PH patients.

Using clinical criteria, PH was defined as mean pulmonary arterial pressure (mPAP) >20 mmHg. Pre-capillary PH was defined as PCWP ≤15 mmHg while post-capillary PH was defined as PCWP >15 mmHg (10). Patients with combined post- and pre-capillary PH [cpc-PH; defined as PCWP >15 mmHg and diastolic pressure gradient (DPG) ≥7 mmHg and/or pulmonary vascular resistance (PVR) >3 Wood units] were classified as "post-capillary PH" in the present study because cpc-PH had a high left heart pressure and was generally thought to evolve from post-capillary PH (11).

MRI scan parameters

Cine MRI scans were performed with a 1.5 T scanner (Magnetom, Aera, SIEMENS, Erlangen, Germany) by clinical technicians in our institution. First, a fast sequence was run to localize anatomic orientation for cardiac structures. Then, two-, three-, and four-chamber, and short-axis orientations of the heart were identified by using a black-blood half-Fourier rapid acquisition with relaxation enhancement sequence. Third, a segmented balanced steady-state free precession (bSSFP) sequence was applied in the two-, three- and four-chamber and short-axis views to acquire cine images. Detailed imaging parameters included: repetition time (TR)/echo time (TE) =35.4/1.1 ms; Echo spacing =1.3 ms; flip angle =65°; bandwidth =930 Hz/pixel; voxel size =2.1×2.1×6.0 mm^3; inter-slice gap =4 mm; generalized autocalibrating partially parallel acquisition (GRAPPA) technique with reduction factor R=2. For each myocardial slice, images (with 25 retrospectively constructed cardiac phases) were obtained during a breath-hold at end-expiration using retrospective electrocardiogram (ECG) gating. The entire LV (from base to apex) was covered by 10 to 14 short-axis slices.

HDA analysis on cine MRI datasets

Image datasets were transferred to a dedicated image processing workstation (HP, EliteDesk 800 G2 TWR). De-identified cine images were processed by an experience analyzer (KL; with 17 years of experience in cardiovascular imaging) using a prototype software of HDA programmed in Visual C++ (TrufiStrain, version 2.0, Siemens Healthcare,

Erlangen, Germany). Based on the deformation inversion recovery (DIR) algorithm that was previously reported, the HDA tool automatically detected cardiac landmarks and defined epicardial and endocardial myocardial borders without manual contour drawing (12). LV end-diastolic volume (LVEDV) and LV end-systolic volume (LVESV) were then acquired. LV stroke volume (LVSV) = LVEDV – LVESV. LV cardiac output (LVCO) was defined as heart rate × LVSV. LV cardiac index (LVCI) was calculated as LVCO/body surface area. The LVEF was calculated as follows: LVEF = (LVSV/LVEDV) × 100. LV myocardial volume was calculated by adding up the LV volume (area × thickness) in each slice between endocardial and epicardial borders at end-diastole. LVM was calculated assuming a myocardial density of 1.05 g/mL (13).

At the same time, HDA calculated motion deformation fields on cine images between any two cardiac time frames for a given LV plane (14). By computing the dense deformation fields and the inverse deformation fields using gradient descent minimization, global and segmental cardiac motion parameters, including displacement (the shortest distance from the initial to the final position of a pixel), velocity (displacement/time), strain [(change in length of an area)/(original length)] and strain rate (changes of strain/time interval) were derived from the variant deformation fields over time. Next, in-plane time-resolved cardiac motion vectors in the radial and circumferential directions were calculated for the entire LV (global values) and for individual LV segments, mapped on an American Heart Association (AHA)—16 segment model (7). The workflow of the HDA was shown in *Figure 1*. Peak motion/deformation indices (along radial and circumferential directions) in early and late diastole were extracted by using existing methods and were expressed with absolute values regardless of motion directions (7).

DL framework structure and training

An artificial neural network (ANN; an algorithm of DL developed by using Keras is built on top of TensorFlow) was developed in Python (version 3.85). This model contained input layer, intermediate hidden layer(s) and the output layer (Softmax). See *Figure 2* for the structure of the model.

Motion/deformation indices from 40 randomly chosen PH patients was used to train and fit the model. The model used "scikit-learn" to estimate the performance of the model. Then, the logarithmic loss function (binary_crossentropy) was applied to estimate the loss of the model so that the weights of every motion/deformation index could be adjusted to improve efficacy of the prediction. Finally, the efficient Adam optimization algorithm for accuracy metrics and gradient descent was obtained. Number of neurons was set to 12 according to HDA generated LV motion/deformation data (including radial and circumferential peak displacement, velocity, strain rate at early and late diastole). The number of "Epoch" (entire dataset passing forward and backward through the neural network) was set to 150. The result of RHC for the diagnosis of PH was set as the "ground truth".

Statistical analysis

The data of other 14 patients were used to test the performance of the DL framework. The running time of the model was recorded. The accuracy, sensitivity, specificity, positive predictive value (PPV) and negative predictive value (NPV) to discriminate post-capillary PH from pre-capillary PH. The receiver operating characteristic (ROC) curve and the area under the curve (AUC) were used to evaluate the diagnosis performance of the DL framework.

Results

The mean interval between RHC and cine MRI was 20.5±5.7 days. Among 54 PH patients, 40 PH patients (18 pre-capillary PH and 22 post-capillary PH) were assigned to the "training" group and the rest 14 patients (8 pre-capillary PH and 6 post-capillary PH) entered the "testing" group. There were no significant differences between demographic information and LV functions between the two groups (training *vs*. testing). See *Table 1*.

Cine MRI-derived peak displacement, velocity and strain rates at early and late diastole (totally 12 items) of 40 PH patients (the "training group") entered the model for training. The accuracy gradually increased while the loss decreased during the modeling training. The prediction accuracy of the final model reached 0.875 (*Figure 3*).

After training, the model was able to correctly identify types of PH in 12 of 14 PH patients (the "testing group"). The time for training and prediction was less than 2 minutes. The accuracy, sensitivity, specificity, PPV and NPV for discriminating post-capillary PH from pre-capillary PH in the "testing group" were 86%, 83%, 88%, 83% and 88%, respectively. See *Table 2*. The AUC was 0.85 [95% confident interval (CI): 0.629–1] (*Figure 4*).

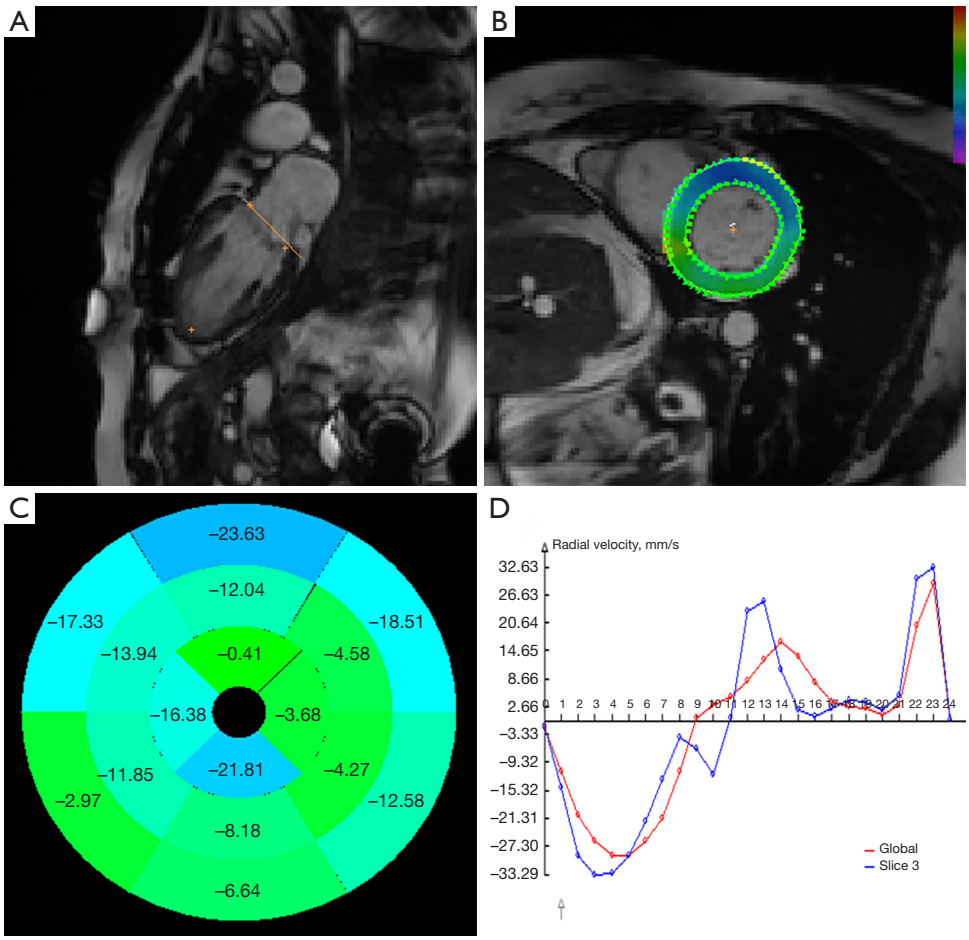

Figure 1 Automatic workflow (after a single click) of the HDA for the extraction of LV motion/deformation indices without manual image segmenting. (A) The anatomic anchor points were automatically detected by HDA. (B) The inner- and outer-borders of the LV were detected by HDA for each slice and each frame at short-axis view. (C) The motion/deformation indices were calculated based on the contours. (D) The time curves were generated for displaying variations of multiple indices through a cardiac cycle. HDA, heart deformation analysis; LV, left ventricular.

Discussion

In the present study, we developed a DL framework to automatically identify elevated left heart pressure in PH patients (discriminating pre- and post-capillary PH) by analyzing HDA-generated LV motion/deformation indices on regular cine MRI datasets.

Currently, echocardiography is the major noninvasive method for the estimation of elevated left heart pressure. Unfortunately, the echocardiographic criteria for the diagnosis of increased LV filling pressure (LVFP) are not straightforward. Many echocardiographic parameters, such as peak early mitral flow velocity (E) to peak early mitral annulus velocity (e'), left atrial (LA) maximum volume index (LAVI) and peak tricuspid regurgitation (TR) should be included and considered together for establishing the diagnosis. Such a set of complicated criteria results from the fact that echocardiographic indices could be influenced by coexisting cardiovascular conditions. For example, the measurements for e' and the E/e' ratio are less accurate when a left bundle branch block (LBBB) exists (15). Santos *et al.* investigated the correlations between the E/e' ratio and PCWP in 118 patients with unexplained dyspnea who underwent both transthoracic echocardiogram (TTE) and RHC. The authors found that the E/e' ratio neither accurately estimates PAWP nor represents changes in PCWP (16). Consequently, even when demographic

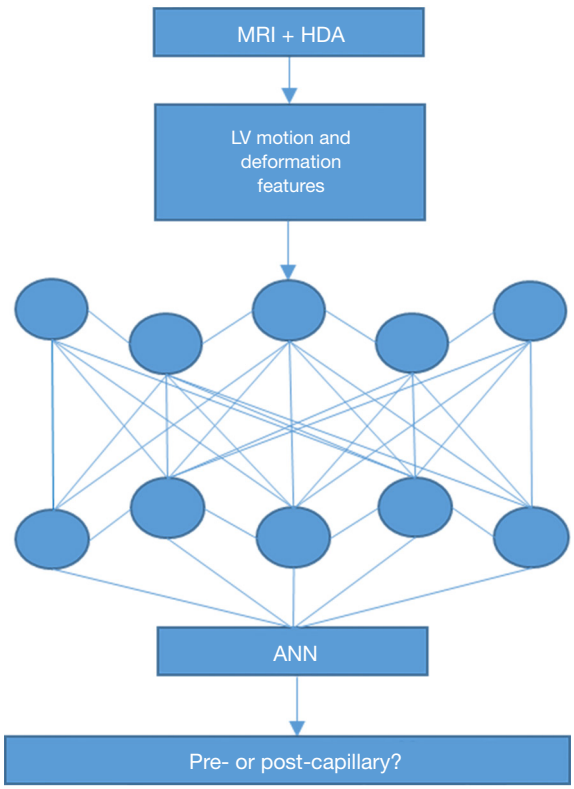

Figure 2 The structure of the DL model. After the image features (acquired with HDA) were input, the ANN provided binary predictions (Softmax function) after model training. DL, deep learning; HDA, heart deformation analysis; ANN, artificial neural network.

information, such as age and other cardiovascular risk conditions, was added to diagnostic algorithms, the echocardiography-centered detection of increased left heart pressure could still be challenging in cases with complicated hemodynamic abnormalities (17,18).

DL is a part of machine learning (ML) that resembles the multilayered human cognition system and facilitates diagnosis and clinical decision making (19). Recently, DL has been widely used in medical imaging processing. One typical task of DL in radiology practice was detecting structural abnormalities and classifying them into disease categories. For example, a DL framework could provide comparable or better accuracy in the diagnosis of breast cancer (20). To date, DL has also been used to detect cardiovascular diseases (CVDs). Ghorbani *et al.* developed a convolutional neural network (CNN) to identify the presence of pacemaker leads (AUC =0.89), enlarged left atrium (AUC =0.86), LV hypertrophy (AUC =0.75), LVEDV and LVESV (R^2=0.74 and R^2=0.70), and LVEF (R^2=0.50) based on echocardiographic images (21). Tao *et al.* developed a CNN to automatically segment cine MRI datasets. The average perpendicular distance compared with manual analysis was 1.1±0.3 mm (22). Zhang *et al.* developed a deep neural network (DNN) to extract the regions of myocardial infarction (MI) within the LV from cine MRI data (23). The authors found that the per-segment sensitivity and specificity for detecting chronic MI in the independent test set was 89.8% and 99.1%, respectively, with an AUC of 0.94.

Generally, a DL framework for the analysis of LV function and motion should contain two components. (I) An imaging processing unit for the detection and segmentation of the LV and extraction of LV motion and deformation features within a cardiac cycle; (II) a discriminative frame network that can identify disorders based on imaging features with or without other clinical information. The HDA-generated LV function, motion and deformation indices have good agreement with other existing tools, including Argus (Siemens healthcare), feature tracking (FT) and tissue phase mapping (TPM) (5,6,24). Therefore, for our DL model, HDA-generated LV motion/deformation indices were directly adopted as the input because HDA is a mature tool for automatic detecting and measuring LV function, motion and deformation features. By omitting component for LV segmentation, our DL model focused on judging the existence of elevated left heart pressure based on output data of HDA. Such an arrangement greatly simplified the structure of the DL model, reduced the amount of calculation and improved the efficacy of the diagnosis in clinical settings.

TensorFlow is a library developed by Google that is widely used for DL applications. Acting as an application programming interface (API), Keras wraps the numerical computation libraries, including Theano and TensorFlow, and allows to build and train DL models with a few lines of code (25). Being a output layer in Keras, softmax function is a generalization of the logistic regression with multiple dimensional information and can provide classification or judgement likelihood (26). Those recent advances in software infrastructure significantly reduced technical thresholds for constructing advanced DL techniques. Combined with the application of HDA, our concise DL model demonstrated its capability for the identification of elevated left heart pressure in clinical PH patients. At the same time, this model may have potential in the diagnosis of

Table 1 Descriptions of the PH patients for "training" and "testing" purposes

Items	Testing (n=14)	Training (n=40)	P values
Age (years), mean ± SD	57.1±11.7	59.5±14.3	0.571
Male, n [%]	3 [21]	20 [50]	0.065
Height (cm), mean ± SD	167.6±7.4	168.6±9.5	0.751
Weight (kg), mean ± SD	69.2±25.9	92.5±22.6	0.66
BMI, mean ± SD	31.5±7.7	32.4±7	0.68
PCWP (mmHg), mean ± SD	14.3±5.6	16.3±6.1	0.289
mPAP (mmHg), mean ± SD	38.6±12.2	35.6±9.9	0.35
PVR (Wood units), mean ± SD	5.6±3.7	4.3±2.6	0.149
LVEF (%), mean ± SD	60.3±11.1	54.6±12.8	0.143
LVM (g), mean ± SD	111.8±34.9	11.1±28.2	0.219
LVEDV (mL), mean ± SD	132.9±42.5	152.1±58.5	0.266
LVESV (mL), mean ± SD	54.9±31.9	73.5±46.3	0.172
LVSV (mL), mean ± SD	78.1±21.5	78.7±26	0.936
LVCO (L/min), mean ± SD	5.5±1.9	5.4±1.7	0.819
LVCI (L/min/m^2), mean ± SD	2.7±0.9	2.6±0.7	0.593

PH, pulmonary hypertension; BMI, body mass index; PCWP, pulmonary capillary wedge pressure; mPAP, mean pulmonary arterial pressure; PVR, pulmonary vascular resistance; LVEF, left ventricular ejection fraction; LVM, left ventricular mass; LVEDV, left ventricular end-diastolic volume; LVESV, left ventricular end-systolic volume; LVSV, left ventricular stroke volume; LVCO, left ventricular cardiac output; LVCI, left ventricular cardiac index.

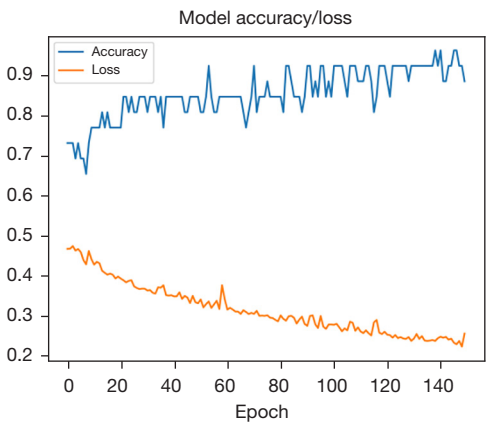

Figure 3 The accuracy of the model increased while the loss decreased during training.

Table 2 The 2×2 table showed the capability of our DL model for the identification of PH types

DL results	Ground truth	
	Pre	Post
Pre	7	1
Post	1	5

The accuracy, sensitivity, specificity, PPV, NPV could be calculated. DL, deep learning; PH, pulmonary hypertension; PPV, positive predictive value; NPV, negative predictive value.

other CVDs with similar pathophysiological changes, such as HFpEF.

Our study has limitations. First, due to limited availability of PH patients, the number of cases for fitting and training model is 40. The small patient pool for model training could lower limit the "proficiency" of the DL model. However, the good accuracy suggested that the DL algorithm's performance is promising. Second, existing HDA software only automatically measured radial and circumferential myocardial motion/deformation indices. Further investigations are needed to explore the clinical relevance of LV diastolic motion indices in the long-axial direction. Third, no intra- and inter-observer agreements

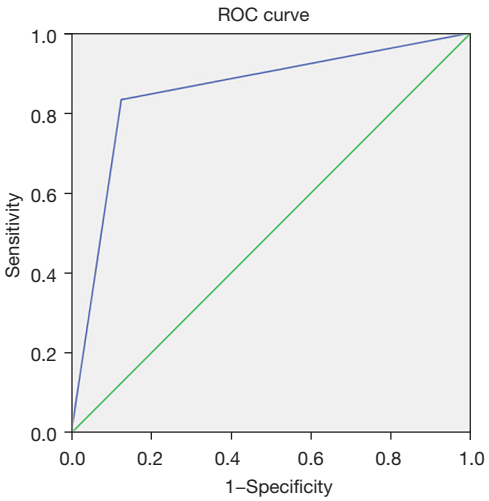

Figure 4 ROC showed performance of our DL model for the discriminating pre-capillary PH from post-capillary PH. The AUC =0.85 (95% CI: 0.629–1). ROC, receiver operating characteristic; DL, deep learning; PH, pulmonary hypertension; AUC, area under the curve; CI, confident interval. Diagonal segments are produced by ties.

were presented in the present study. RHC is a mature procedure and the pressure measurements have been adopted as the "reference standard" in clinical practice. HDA is an operator-independent tool. For each given cine dataset, the HDA always generates the same set of outputs. The agreements between HDA and similar approaches, such as TPM and FT, for describing cardiac motion/deformation patterns have been reported in previous publications (2,5-8,24).

In conclusion, DL can identify elevated left heart pressure underlying post-capillary PH based on LV motion/deformation patterns presented on regular cine MRI datasets.

Acknowledgments

Funding: This study was partly supported by grants from the National Institute of Health (K01HL121162 and R03HL144891 to KL). This study was partly supported by Bayer pharmaceutical. The grant was paid to the institution, not to individual researchers.

Footnote

Reporting Checklist: The authors have completed the STARD reporting checklist. Available at https://jmai.amegroups.com/article/view/10.21037/jmai-21-27/rc

Data Sharing Statement: Available at https://jmai.amegroups.com/article/view/10.21037/jmai-21-27/dss

Conflicts of Interest: All authors have completed the ICMJE uniform disclosure form (available at https://jmai.amegroups.com/article/view/10.21037/jmai-21-27/coif). KL was supported by grants from the National Institutes of Health (K01HL121162 and R03HL144891). JCC receives institutional research grant from Siemens, Bayer and Guerbet, speaker honoraria from Bayer and is on advisory boards for Siemens, Bayer and Bracco. The other authors have no conflicts of interest to declare.

Ethical Statement: The authors are accountable for all aspects of the work in ensuring that questions related to the accuracy or integrity of any part of the work are appropriately investigated and resolved. The study was conducted in accordance with the Declaration of Helsinki (as revised in 2013). The study was approved by the institution review board of Northwestern University (STU00205106). Written informed consents were provided by all participants before MRI scans.

References

1. Glowny MG, Resnic FS. Cardiology patient page. What to expect during cardiac catheterization. Circulation 2012;125:e363-4.
2. Lin K, Sarnari R, Pathrose A, et al. Cine MRI characterizes HFpEF and HFrEF in post-capillary pulmonary hypertension. Eur J Radiol 2021;139:109679.
3. Jerosch-Herold M, Kwong RY. Magnetic resonance imaging in the assessment of ventricular remodeling and viability. Curr Heart Fail Rep 2008;5:5-10.
4. de Roos A, Higgins CB. Cardiac radiology: centenary

review. Radiology 2014;273:S142-59.
5. Lin K, Collins JD, Chowdhary V, et al. Heart deformation analysis for automated quantification of cardiac function and regional myocardial motion patterns: A proof of concept study in patients with cardiomyopathy and healthy subjects. Eur J Radiol 2016;85:1811-7.
6. Lin K, Collins JD, Chowdhary V, et al. Heart deformation analysis: measuring regional myocardial velocity with MR imaging. Int J Cardiovasc Imaging 2016;32:1103-11.
7. Lin K, Ma H, Sarnari R, et al. Cardiac MRI Reveals Late Diastolic Changes in Left Ventricular Relaxation Patterns During Healthy Aging. J Magn Reson Imaging 2021;53:766-74.
8. Lin K, Sarnari R, Pathrose A, et al. Cine MRI detects elevated left heart pressure in pulmonary hypertension. J Magn Reson Imaging 2021;54:275-83.
9. Liu X, Faes L, Kale AU, et al. A comparison of deep learning performance against health-care professionals in detecting diseases from medical imaging: a systematic review and meta-analysis. Lancet Digit Health 2019;1:e271-97.
10. Rosenkranz S, Preston IR. Right heart catheterisation: best practice and pitfalls in pulmonary hypertension. Eur Respir Rev 2015;24:642-52.
11. Guazzi M, Borlaug BA. Pulmonary hypertension due to left heart disease. Circulation 2012;126:975-90.
12. Jolly MP, Guetter C, Lu X, et al. Automatic segmentation of the myocardium in cine MR images using deformable registration. In: International workshop on statistical atlases and computational models of the heart. Berlin, Heidelberg: Springer, 2011:98-108.
13. Montant P, Chenot F, Goffinet C, et al. Detection and quantification of myocardial scars by contrast-enhanced 3D echocardiography. Circ Cardiovasc Imaging 2010;3:415-23.
14. Guetter C, Xue H, Chefd'Hotel C, et al. Efficient symmetric and inverse-consistent deformable registration through interleaved optimization. In: 2011 IEEE international symposium on biomedical imaging: from nano to macro. IEEE, 2011:590-3.
15. Nagueh SF, Bhatt R, Vivo RP, et al. Echocardiographic evaluation of hemodynamics in patients with decompensated systolic heart failure. Circ Cardiovasc Imaging 2011;4:220-7.
16. Santos M, Rivero J, McCullough SD, et al. E/e' Ratio in Patients With Unexplained Dyspnea: Lack of Accuracy in Estimating Left Ventricular Filling Pressure. Circ Heart Fail 2015;8:749-56.
17. Pieske B, Tschöpe C, de Boer RA, et al. How to diagnose heart failure with preserved ejection fraction: the HFA-PEFF diagnostic algorithm: a consensus recommendation from the Heart Failure Association (HFA) of the European Society of Cardiology (ESC). Eur Heart J 2019;40:3297-317.
18. Reddy YNV, Carter RE, Obokata M, et al. A Simple, Evidence-Based Approach to Help Guide Diagnosis of Heart Failure With Preserved Ejection Fraction. Circulation 2018;138:861-70.
19. Lee JG, Jun S, Cho YW, et al. Deep Learning in Medical Imaging: General Overview. Korean J Radiol 2017;18:570-84.
20. McKinney SM, Sieniek M, Godbole V, et al. International evaluation of an AI system for breast cancer screening. Nature 2020;577:89-94.
21. Ghorbani A, Ouyang D, Abid A, et al. Deep learning interpretation of echocardiograms. NPJ Digit Med 2020;3:10.
22. Tao Q, Yan W, Wang Y, et al. Deep Learning-based Method for Fully Automatic Quantification of Left Ventricle Function from Cine MR Images: A Multivendor, Multicenter Study. Radiology 2019;290:81-8.
23. Zhang N, Yang G, Gao Z, et al. Deep Learning for Diagnosis of Chronic Myocardial Infarction on Nonenhanced Cardiac Cine MRI. Radiology 2019;291:606-17.
24. Lin K, Collins JD, Lloyd-Jones DM, et al. Automated Assessment of Left Ventricular Function and Mass Using Heart Deformation Analysis: Initial Experience in 160 Older Adults. Acad Radiol 2016;23:321-5.
25. Bharati S, Podder P, Mondal MRH. Hybrid deep learning for detecting lung diseases from X-ray images. Inform Med Unlocked 2020;20:100391.
26. Zhang W, Chen Y, Yang W, et al. Class-Variant Margin Normalized Softmax Loss for Deep Face Recognition. IEEE Trans Neural Netw Learn Syst 2021;32:4742-7.

doi: 10.21037/jmai-21-27
Cite this article as: Lin K, Sarnari R, Pathrose A, Gordon DZ, Markl M, Carr JC. Deep learning for the identification of pre- and post-capillary pulmonary hypertension on cine MRI. J Med Artif Intell 2022;5:2.